Numerical studies of edge localized instabilities in tokamaks

H. R. Wilson
EURATOM/UKAEA Fusion Association, Culham Science Centre, Abingdon, Oxon OX14 3DB, United Kingdom

P. B. Snyder
General Atomics, San Diego, California 92186-5608

G. T. A. Huysmans
Association EURATOM-CEA sur la Fusion, CEA Cadarache, F-13108 St Paul lez Durance, France

R. L. Miller
Archimedes Technology Group, 5405 Oberlin Dr., San Diego, California 92121

(Received 16 November 2001; accepted 15 January 2002)

A new computational tool, edge localized instabilities in tokamaks equilibria (ELITE), has been developed to help our understanding of short wavelength instabilities close to the edge of tokamak plasmas. Such instabilities may be responsible for the edge localized modes observed in high confinement H-mode regimes, which are a serious concern for next step tokamaks because of the high transient power loads which they can impose on divertor target plates. ELITE uses physical insight gained from analytic studies of peeling and ballooning modes to provide an efficient way of calculating the edge ideal magnetohydrodynamic stability properties of tokamaks. This paper describes the theoretical formalism which forms the basis for the code. [DOI: 10.1063/1.1459058]

I. INTRODUCTION

In the high confinement H-mode of tokamak operation, a transport barrier forms at the plasma edge, leading to a steep pressure gradient, and therefore, a high bootstrap current. High pressure gradients can lead to high toroidal mode number, n, ballooning instabilities (e.g., see Ref. 1) but, on the other hand, high edge current reduces the magnetic shear which helps to stabilize these. However, high edge currents can drive high n kink or ''peeling'' modes,[2–4] and these are stabilized by edge pressure gradient (due to the effect of favorable average curvature in a tokamak). This interplay between pressure and current makes edge stability particularly interesting. As a final ''twist'' to the story, the ballooning and peeling modes can couple,[5] leading to particularly dangerous current-driven instabilities which can extend right across the transport barrier region, into the plasma core.[4] The result is that a range of instabilities can exist from highly localized peeling modes, more extended ballooning modes, extended, coupled peeling-ballooning modes, or, indeed, access to a second stability region[6] with correspondingly higher pressure gradient limits. This range of possible ideal magnetohydrodynamic (MHD) plasma edge instabilities may help to explain the wide range of edge localized mode (ELM) phenomena observed in tokamaks, such as relatively small type III ELMs at low pressure gradient, up to large type I ELMs, smaller ''grassy'' ELMs or even ELM-free regimes at larger pressure gradient (for a review of ELM phenomenology, see Ref. 7). Understanding these instabilities may then help us to identify how to access regimes which have tolerable ELMs: A key issue for the International Thermonuclear Experimental Reactor (ITER).[8] It is, therefore, important to be able to analyze these instabilities, which is complicated by their short wavelength (much shorter than the typical equilibrium length scales) and two-dimensional nature. In this paper we describe a formalism which permits efficient analysis of this class of instabilities within a linearized ideal MHD model.

The paper is set out as follows. In the next section we describe the formalism which we have developed for analyzing high n, coupled peeling-ballooning modes in tokamaks. The technique is applicable to arbitrary tokamak equilibria, except that at present we have not considered the separatrix. Then, in Sec. III, we illustrate some results from the code, which we have called ELITE (Edge Localized Instabilities in Tokamak Equilibria). We first describe a benchmark case, which we take to be a circular cross section, aspect ratio $A=3$ plasma which has an edge pressure pedestal unstable to $n=\infty$ ballooning modes. We compare the results of ELITE with those of MISHKA-1,[9] and find good agreement for $n>4$ (ELITE makes use of an expansion for large n). Next we illustrate the results for a shaped plasma equilibrium, in this case a DIII-D equilibrium re-constructed using EFIT.[10] In Sec. IV we draw some conclusions, and make some suggestions for how the model could be further improved.

II. ELITE FORMALISM

To help improve the efficiency of ELITE we restrict consideration to intermediate to high n modes, and evaluate the change in energy associated with a radial perturbation of a plasma fluid element, denoted by X. Following Ref. 1, we perform an expansion in n^{-1}, which permits the other two components of plasma perturbation to be eliminated in favor of X. After some algebra, neglecting the contribution due to

Downloaded 14 Feb 2006 to 198.129.105.159. Redistribution subject to AIP license or copyright, see http://pop.aip.org/pop/copyright.jsp

the inertia for the present, it can be shown that the change in energy, correct to the first two orders in n^{-1} can be written in the form

$$\delta W=\pi\int_{-\infty}^{0}d\psi\oint d\chi\left\{\frac{JB^2}{R^2B_p^2}|k_\parallel X|^2+\frac{R^2B_p^2}{JB^2}\left|\frac{1}{n}\frac{\partial Y}{\partial\psi}\right|^2-\frac{2Jp'}{B^2}\left[|X|^2\frac{\partial}{\partial\psi}\left(p+\frac{B^2}{2}\right)-\frac{i}{2}\frac{f}{JB^2}\frac{\partial B^2}{\partial\chi}\frac{X^*}{n}\frac{\partial X}{\partial\psi}\right]-\frac{X^*}{n}JBk_\parallel(\sigma' X)+\frac{1}{n}[PJBk_\parallel^*Q^*+P^*JBk_\parallel Q]+\frac{\partial}{\partial\psi}\left[\frac{\sigma}{n}X^*Y\right]\right\}. \tag{1}$$

Here we have defined the poloidal magnetic flux, ψ, and toroidal field function, $f(\psi)$, such that the magnetic field can be expressed in the form

$$\boldsymbol{B}=f\boldsymbol{\nabla}\phi+\boldsymbol{\nabla}\phi\times\boldsymbol{\nabla}\psi, \tag{2}$$

so that ψ is an increasing function of the minor radius of flux surfaces. We have chosen the gauge for ψ such that $\psi=0$ at the plasma edge, and takes a negative value everywhere in the core. In fact, because we are interested in edge localized modes, whose amplitude $X\to 0$ in the core, we can replace the lower limit of integration in the ψ variable by $-\infty$, as indicated in Eq. (1). The orthogonal (ψ,χ,ϕ) coordinate system we use is similar to that used in Ref. 1, where χ is a poloidal angle and ϕ the toroidal angle; J is the Jacobian in this system, defined such that $Jd\chi=dl/B_p$, where dl is the poloidal arc length element along a flux surface, and B_p is the poloidal component of the magnetic field. The major radius is denoted by R and B is the total magnetic field. The pressure (with a factor μ_0 absorbed) is denoted by p, a prime denotes a differential with respect to ψ and a star denotes a complex conjugate. The variable Y is simply related to X

$$Y=JBk_\parallel X, \tag{3}$$

where the parallel gradient operator is defined by

$$JBk_\parallel=-i\frac{\partial}{\partial\chi}+n\nu, \tag{4}$$

with

$$\nu=\frac{fJ}{R^2}. \tag{5}$$

The parallel current density, denoted by σ, can be written in the form

$$\sigma=-\frac{fp'}{B^2}-f'. \tag{6}$$

Finally, P and Q are defined as

$$P=\sigma X+\frac{fB_p^2}{n\nu B^2}\frac{\partial Y}{\partial\psi}, \tag{7}$$

$$Q=\frac{p'}{B^2}X+\frac{f}{JB^2}\frac{1}{n}\frac{\partial Y}{\partial\psi}. \tag{8}$$

Note that Eq. (1) involves contributions to δW due to surface terms arising from integrations by parts. These were absent in the ballooning analysis of core modes developed in Ref. 1, because there the mode amplitude was assumed to be negligible at the plasma–vacuum interface. It is important to retain these in our situation as the mode amplitude is not negligible at the plasma boundary, and indeed is an essential feature of the peeling modes which we wish to analyze. Also note that by retaining terms up to, and including, $O(n^{-1})$ we retain the kink drive, proportional to the radial derivative of the parallel current density.

The above expression (1) neglects the inertial energy. Although we are primarily interested in marginal stability, it is useful to have an indication of the growth rate, so we employ a simplified model which neglects that inertia associated with displacements parallel to the magnetic field (equivalent to the assumption of incompressible MHD, valid at marginal stability). Thus, for the inertial energy, we derive

$$\delta W_I=\pi\gamma^2\int_{-\infty}^{0}d\psi\oint d\chi\left\{\frac{\rho J}{R^2B_p^2}|X|^2+\frac{\rho JR^2B_p^2}{n^2B^2}\left|\frac{\partial X}{\partial\psi}\right|^2+\frac{G}{n^2}\left(X\frac{\partial X^*}{\partial\psi}+X^*\frac{\partial X}{\partial\psi}\right)+\frac{H}{n^3}\left(\frac{\partial X^*}{\partial\psi}JBk_\parallel\left(\frac{\partial X}{\partial\psi}\right)+\frac{\partial X}{\partial\psi}JBk_\parallel^*\left(\frac{\partial X^*}{\partial\psi}\right)\right)\right\}. \tag{9}$$

The equilibrium functions H and G are defined in Eqs. (A4) and (A5) of Appendix A, $\rho(\psi)$ is the mass density and γ^2 is the eigenvalue of the system, equal to the square of the growth rate. Again, within our "incompressible MHD" model, the inertia term is correct to the first two orders in n^{-1}.

Note that we have performed an ordering in n^{-1} so that the Hermitian property of ideal MHD is exactly preserved; we find this to be important for the numerical results.

The method is now straightforward, but involves a large amount of tedious algebra. We first Fourier decompose the poloidal variation of the displacement X, and it is convenient to do this in terms of a "straight field line" angle, ω

$$\omega=\frac{1}{q}\int^{\chi}\nu d\chi, \tag{10}$$

where the safety factor q is simply $q=(1/2\pi)\oint\nu d\chi$. Thus we express

$$X=\sum_m u_m(x)e^{-im\omega}, \tag{11}$$

where m are the poloidal mode numbers, and then we have

$$Y=\sum_m\left(-\frac{\nu}{q}\right)(m-nq)u_m(x)e^{-im\omega}. \tag{12}$$

For high m modes field line bending will have a strong influence, and will tend to restrict the u_m to be localized about their mode rational surfaces, where $m=nq$. Thus we have introduced the "fast" radial variable

$$x=m_0-nq, \tag{13}$$

Downloaded 14 Feb 2006 to 198.129.105.159. Redistribution subject to AIP license or copyright, see http://pop.aip.org/pop/copyright.jsp

which is the length scale on which we expect the u_m to vary. Here m_0 is the poloidal mode number of some reference rational surface, and we arbitrarily choose it to be that associated with the first rational surface in the vacuum, i.e.,

$$m_0 = \mathrm{Int}[nq_a] + 1, \tag{14}$$

where q_a is the edge safety factor. Note that x increases by 1 each time a rational surface is crossed as we go from the plasma edge towards the core.

We now substitute the forms for X and Y into Eqs. (1) and (9), and perform integrations by parts (in the radial coordinate) to eventually derive a form for δW, which can be decomposed into a contribution from the core plasma, δW_p, and a piece arising from the surface terms due to the integrations by parts, δW_s

$$\delta W = \delta W_p + \delta W_s. \tag{15}$$

For our vacuum model we assume that the vessel wall is far from the plasma, so that it is effectively surounded by an infinite vacuum on all sides; this is a good approximation for the radially localized modes which we consider. In such a situation the vacuum contribution to δW can be expressed analytically solely in terms of the plasma displacement at the plasma–vacuum interface,[11] and therefore, can be absorbed into δW_s. The resulting expressions for δW_p and δW_s are given in Appendix A.

We stress here that ELITE is not based on a δW numerical approach, but instead solves the full set of Euler equations for the radial variations of the Fourier mode amplitudes. These can be derived trivially from Eq. (A1), and for each Fourier mode k they take the form

$$\begin{aligned}
\sum_m \Big\{ & [A''^{k,m}_{2mk}(m-nq)^2(k-nq) + A''^{k,m}_{m2k}(m-nq)(k-nq)^2 + A''^{k,m}_{mk}(m-nq)(k-nq) - \gamma^2(I''^{k,m}_m(m-nq) + I''^{k,m}_k(k-nq) \\
& + I''^{k,m})]\frac{d^2u_m}{d\psi^2} + [A'^{k,m}_{2mk}(m-nq)^2(k-nq) + A'^{k,m}_{m2k}(m-nq)(k-nq)^2 + A'^{k,m}_{mk}(m-nq)(k-nq) + A'^{k,m}_{2m}(m-nq)^2 \\
& + A'^{k,m}_{2k}(k-nq)^2 + (A'^{k,m}_m - \gamma^2 I'^{k,m}_m)(m-nq) + (A'^{k,m}_k - \gamma^2 I'^{k,m}_k)(k-nq) + A'^{k,m} - \gamma^2 I'^{k,m}]\frac{du_m}{d\psi} \\
& + [A^{k,m}_{2mk}(m-nq)^2(k-nq) + A^{k,m}_{m2k}(m-nq)(k-nq)^2 + A^{k,m}_{mk}(m-nq)(k-nq) + A^{k,m}_{2m}(m-nq)^2 + A^{k,m}_{2k}(k-nq)^2 \\
& + (A^{k,m}_m - \gamma^2 I^{k,m}_m)(m-nq) + (A^{k,m}_k - \gamma^2 I^{k,m}_k)(k-nq) + A^{k,m} - \gamma^2 I^{k,m}]u_m \Big\} = 0,
\end{aligned} \tag{16}$$

where the matrix elements $A^{k,m}$, $A'^{k,m}$, and $A''^{k,m}$ are given in Appendix A, together with those associated with the inertia, labeled by I. Note that the number of primes on the matrix elements is used as a notation to indicate the number of ''radial'' derivatives on their associated Fourier amplitudes u_m, and does not represent a ψ-derivative of the matrix elements themselves here (superscripts label the matrix elements).

If we assume that some number, M, of Fourier harmonics is required to describe the modes, then Eq. (16) represents a system of M coupled, linear differential equations for the mode amplitudes, u_m. To complete the specification of the system we need to provide a set of boundary conditions. The first of these is that the $u_m(x)$ tend to zero deep inside the plasma core (i.e., we are interested only in edge-localized modes); thus we have

$$\lim_{x\to\infty} u_m(x) = 0. \tag{17}$$

Another boundary condition is that the surface contribution to the total energy must be zero, which represents the fact that the jump in $p + B^2/2$ across the plasma–vacuum interface is zero.[11] The final matching condition, that the radial component of the magnetic field is continuous across the interface, is used to express the vacuum magnetic-field perturbation in terms of the u_m at the plasma surface. Thus we arrive at a second set of conditions (for each k) to be applied at the plasma boundary, $x = \Delta = m_0 - nq_a$, where $0 \leqslant \Delta \leqslant 1$

$$\begin{aligned}
\sum_m \Big\{ & [S'^{k,m}_{2mk}(m-nq)^2(k-nq) + S'^{k,m}_{m2k}(m-nq)(k-nq)^2 + S'^{k,m}_{mk}(m-nq)(k-nq) - \gamma^2(J'^{k,m}_m(m-nq) \\
& + J'^{k,m}_k(k-nq) + J')]\frac{du_m}{d\psi} + [S^{k,m}_{2mk}(m-nq)^2(k-nq) + S^{k,m}_{m2k}(m-nq)(k-nq)^2 + S^{k,m}_{mk}(m-nq)(k-nq) + S^{k,m}_{2k}(k-nq)^2 \\
& + S^{k,m}_k(k-nq) - \gamma^2(J^{k,m}_m(m-nq) + J^{k,m}_k(k-nq) + J^{k,m})]u_m + \delta W^{k,m}_v u_m \Big\}_{x=\Delta} = 0.
\end{aligned} \tag{18}$$

Downloaded 14 Feb 2006 to 198.129.105.159. Redistribution subject to AIP license or copyright, see http://pop.aip.org/pop/copyright.jsp

Again, the matrix elements S and J are defined in Appendix A, and $\delta W_v^{k,m}$ represents the contribution from the vacuum.

The set of Eqs. (16)–(18) constitutes the complete eigenmode system that ELITE has been designed to solve, either to determine whether or not a given configuration is stable, or to find the growth rate of the instability through calculating the eigenvalue γ^2. There are, however, a number of features that greatly increase the efficiency of the code and are worthwhile noting. First there is a separation of equilibrium and mode-structure length scales. Because the equilibrium-varies slowly on a length scale of the order of the distance between rational surfaces (for intermediate to high n) the matrix elements can be evaluated and tabulated on a relatively coarse radial mesh. The Fourier modes, $u_m(x)$, on the other hand, vary on the length scale comparable to the distance between rational surfaces, and these need a much finer radial grid. A second feature of ELITE is that it makes use of the fact that we expect each $u_m(x)$ to be highly localized about its rational surface [i.e., where $m=nq(\psi)$] due to field line bending. This means that while many harmonics may be important to reconstruct the full mode structure, at any one radial position only a limited subset of these will be significant, and the rest can be set to zero amplitude. This provides a significant saving of both computing memory and time.

A final feature of ELITE is how it is designed to evaluate radial derivatives of equilibrium quantities. In principle these can be calculated numerically if the equilibrium is known at all flux surfaces. However, by making use of an expansion of the Grad–Shafranov equation about a flux surface, these derivatives can be calculated analytically in terms of quantities only on that flux surface[12] [specifically the flux surface shape, the poloidal field variation on the flux surface and the profiles $p(\psi)$ and $f(\psi)$ are all that are required]. We require second derivatives (e.g., of the safety factor q) with respect to ψ here, and therefore, we need to expand to higher order than is usually done: The results are presented in Appendix B.

III. NUMERICAL RESULTS

In this section we illustrate some of the results from ELITE. Here we restrict consideration to general results, and will describe more specific tokamak edge stability studies elsewhere.

We begin by considering the stability of a simple aspect ratio, $A=3$, circular cross section tokamak. We have constructed a $\beta_N=2.1$ equilibrium with a steep pressure pedestal at the plasma boundary (see Fig. 1) so that it is unstable to $n=\infty$ ballooning modes in the region $\psi/\psi_a>0.82$, where ψ_a is the poloidal flux at the plasma boundary ($\beta_N=\beta(\%)a(\mathrm{m})B(\mathrm{T})/I_p(\mathrm{MA})$ where β is the ratio of thermal to magnetic pressure, a is the minor radius, B is the magnetic field and I_p is the plasma current). The current profile is calculated from neoclassical theory, assuming a constant loop voltage across the plasma, and allowing for the bootstrap current. Figure 1(b) shows the profile of the plasma current density; note that it is strongly peaked on axis, which is a consequence of neoclassical conductivity, but that there is significant current driven in the pedestal region, due mainly to the bootstrap current.

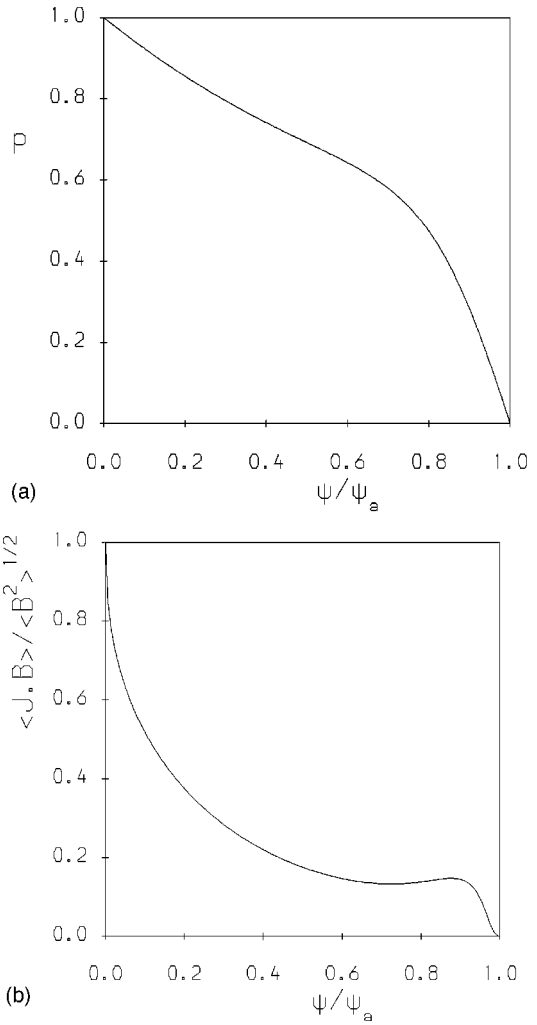

FIG. 1. (a) Pressure profile and (b) current profile for the circular cross-section benchmark study.

Analyzing the stability of the equilibrium, we find that ELITE predicts instability over a range of n. Figure 2 shows a typical mode structure, in this case for a $n=10$ ballooning mode. In Fig. 2(a) we show the set of curves for the $u_m(\psi)$, which illustrates the feature that each harmonic is more radially localized (about its rational surface) than the whole mode structure. Note that in this case the mode is essentially localized within the steep pressure gradient region at the plasma edge [compare with Fig. 1(a)]. In Fig. 2(b) we show the mode structure in poloidal cross section, where we see a clear ballooning mode structure.

Going to higher toroidal mode number, $n=50$, the mode becomes much more radially localized, as expected from conventional ballooning mode theory (e.g., see Ref. 1). This can be seen by comparing Fig. 3, which shows the radial profiles of the Fourier mode amplitudes for this case, with Fig. 2(a).

Using the circular cross-section equilibrium as an example, we have performed a careful benchmark with the MISHKA-1 code,[9] which is also capable of analyzing high n ideal MHD stability. In Fig. 4 we compare the predictions for

Downloaded 14 Feb 2006 to 198.129.105.159. Redistribution subject to AIP license or copyright, see http://pop.aip.org/pop/copyright.jsp

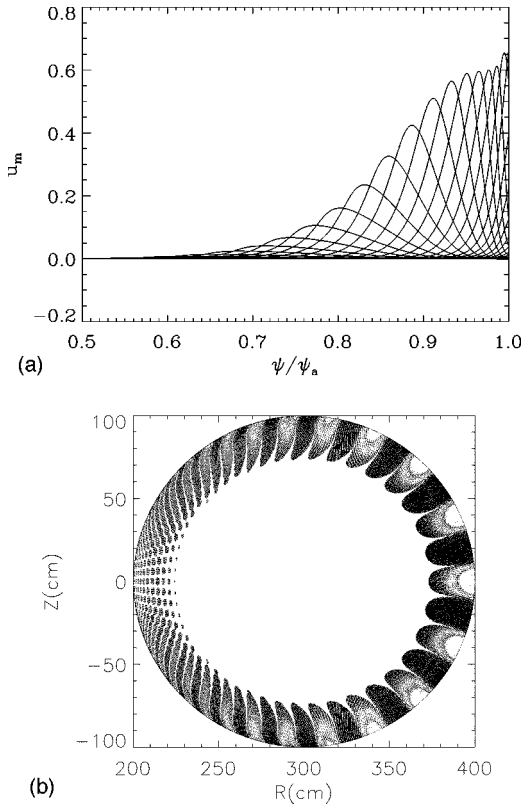

FIG. 2. (a) The radial profiles of the Fourier harmonics $u_m(\psi)$ and a contour plot of the eigenfunction, $X(\psi,\chi)$, for an $n=10$ instability in the circular cross section, $A=3$ equilibrium described in the text. In the contour plot, light and dark shades represent large positive and negative perturbations, respectively.

the growth rates as a function of n from the two codes, and obtain good agreement over the full range of $n \gtrsim 4$. Recall that ELITE is based on an expansion in n^{-1}, while MISHKA-1 is valid over the full range of n. This comparison indicates that ELITE remains valid over the range of intermediate to high n, which is the range of interest for studies of ELMs.

As a final example, we show in Fig. 5 the mode structure in the poloidal cross section of a DIII-D VH-mode discharge (#97887), just before an ELM occurred. In this case the equilibrium is taken from a high resolution, well-converged EFIT

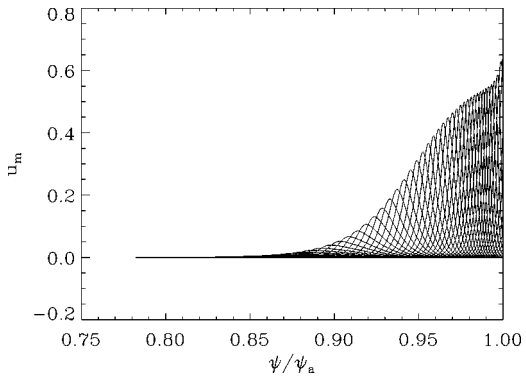

FIG. 3. The radial profiles of the Fourier harmonics for an $n=50$ ballooning mode for the circular cross-section equilibrium.

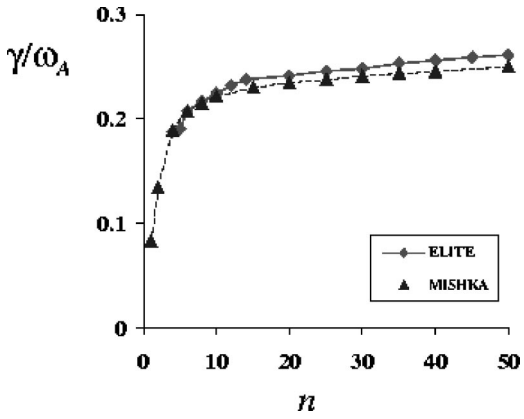

FIG. 4. Comparison between ELITE (diamonds) and MISHKA-1 (triangles) of the growth rate for ideal MHD instabilities in the circular cross-section tokamak (ω_A is the Alfvén frequency).

reconstruction of the discharge, limited at the 99% flux surface (recall that ELITE cannot yet handle the separatrix itself, but can approach it very closely). Note the extremely large number of poloidal harmonics required to analyze these shaped equilibria (compare with Figs. 2 and 3 for the circular cross-section case); ELITE is designed to efficiently handle such cases ($\sim$ minute time scales on $\sim$1 GHz computers).

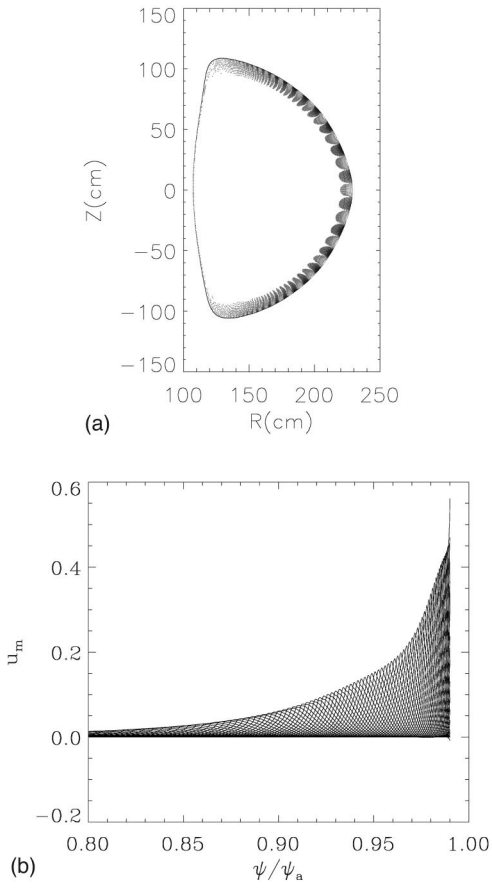

FIG. 5. (a) A contour plot of the eigenfunction, $X(\psi,\chi)$, and (b) the radial profiles of the dominant Fourier amplitudes for an $n=20$ ballooning-type instability in a DIII-D equilibrium (shot #97887).

Downloaded 14 Feb 2006 to 198.129.105.159. Redistribution subject to AIP license or copyright, see http://pop.aip.org/pop/copyright.jsp

IV. CONCLUSIONS

Using our knowledge of the physics underlying ballooning and peeling modes, we have developed a new, efficient tool for calculating the ideal MHD stability of the tokamak plasma edge region, which is often two-dimensional in nature. It is anticipated that this will be useful for helping our understanding of ELMs; in particular, how to control them and how to identify regimes with benign ELMs. In addition, ELITE is useful for calculating the pressure limits that can exist in the edge pedestal region, which is an important ingredient for determining the temperature pedestal (which influences the confinement time).[13] The use of the code to interpret ELMs and the temperature pedestal will be described elsewhere.[14]

This work represents a first step to develop a tool for understanding the stability of tokamak edge plasmas, and as such represents the simplest, useful model of edge plasma stability, ie ideal MHD. There are a number of other features which one could consider incorporating into the model, and these are being considered. One issue is to improve the plasma geometry, allowing for the presence of a separatrix, and even a scrape-off layer plasma, where the field lines connect to material surfaces. The scrape-off layer might be expected to be important when its width is comparable to the linear radial mode width, and could be incorporated into ELITE through modified boundary conditions. Improved plasma physics models would also help us to understand the different ELM regimes observed in more detail. For example, it is likely that diamagnetic effects will be important in the steep gradient regions of the edge transport barrier,[15–17] and also strong sheared plasma flows, as measured in H-mode, might be expected to have an impact on the radially extended, ballooning-type modes. ELITE has been developed in such a way that these improvements could be incorporated as the models are developed.

ACKNOWLEDGMENTS

This work was supported by the U.K. Department of Trade and Industry and EURATOM, and U.S. DOE contract No. DE-FG03-95ER54309.

APPENDIX A: ELITE MATRIX ELEMENTS

The Euler equations and their boundary conditions are derived from the plasma and surface contributions to the perturbed energy, respectively. In terms of the Fourier mode amplitudes, defined through Eq. (11), these can be written in the form

$$\delta W_p=\pi\int_{-\infty}^{\psi_a}d\psi\sum_{m,k}u_k^*\Big\{[A_{2mk}''^{k,m}(m-nq)^2(k-nq)+A_{m2k}''^{k,m}(m-nq)(k-nq)^2+A_{mk}''^{k,m}(m-nq)(k-nq)-\gamma^2(I_m''^{k,m}(m-nq)$$
$$+I_k''^{k,m}(k-nq)+I''^{k,m})]\frac{d^2u_m}{d\psi^2}+[A_{2mk}'^{k,m}(m-nq)^2(k-nq)+A_{m2k}'^{k,m}(m-nq)(k-nq)^2+A_{mk}'^{k,m}(m-nq)(k-nq)$$
$$+A_{2m}'^{k,m}(m-nq)^2+A_{2k}'^{k,m}(k-nq)^2+(A_m'^{k,m}-\gamma^2I_m'^{k,m})(m-nq)+(A_k'^{k,m}-\gamma^2I_k'^{k,m})(k-nq)+A'^{k,m}$$
$$-\gamma^2I'^{k,m}]\frac{du_m}{d\psi}+[A_{2mk}^{k,m}(m-nq)^2(k-nq)+A_{m2k}^{k,m}(m-nq)(k-nq)^2+A_{mk}^{k,m}(m-nq)(k-nq)+A_{2m}^{k,m}(m-nq)^2$$
$$+A_{2k}^{k,m}(k-nq)^2+(A_m^{k,m}-\gamma^2I_m^{k,m})(m-nq)+(A_k^{k,m}-\gamma^2I_k^{k,m})(k-nq)+A^{k,m}-\gamma^2I^{k,m}]u_m\Big\}, \tag{A1}$$

for the plasma contribution, and

$$\delta W_s=\frac{\pi}{n}\sum_{m,k}u_k^*\Big\{[S_{2mk}'^{k,m}(m-nq)^2(k-nq)+S_{m2k}'^{k,m}(m-nq)(k-nq)^2+S_{mk}'^{k,m}(m-nq)(k-nq)-\gamma^2(J_m'^{k,m}(m-nq)$$
$$+J_k'^{k,m}(k-nq)+J')]\frac{du_m}{d\psi}+[S_{2mk}^{k,m}(m-nq)^2(k-nq)+S_{m2k}^{k,m}(m-nq)(k-nq)^2+S_{mk}^{k,m}(m-nq)(k-nq)$$
$$+S_{2k}^{k,m}(k-nq)^2+S_k^{k,m}(k-nq)-\gamma^2(J_m^{k,m}(m-nq)+J_k^{k,m}(k-nq)+J^{k,m})]u_m+\delta W_v^{k,m}u_m\Big\}, \tag{A2}$$

for the surface contribution (where quantities are to be evaluated at the plasma surface). The vacuum contribution is represented by the terms $\delta W_v^{k,m}$

The matrix elements which appear in the above two contributions to the plasma energy and also the set of Euler equations for the radial variation of the Fourier mode amplitudes solved by ELITE, Eq. (16), are given by

$$A^{k,m}=-2\frac{p'q}{f}T_9^{k,m}+qp'\frac{m}{n}T_{11}^{k,m}-\frac{imq'}{n^2q}T_{24}^{k,m}$$
$$-\frac{imq'}{n^2q}T_{26}^{k,m}+\frac{iq}{n}T_{30}^{k,m},$$

Downloaded 14 Feb 2006 to 198.129.105.159. Redistribution subject to AIP license or copyright, see http://pop.aip.org/pop/copyright.jsp

$$A_k^{k,m}=\frac{2mq'}{n^2q^2}T_3^{k,m}+\frac{m}{n^2q^2}\left(q''-2\frac{q'^2}{q}\right)T_4^{k,m}$$
$$-\frac{2im^2q'}{n^2q^2}T_6^{k,m}+\frac{mq'}{n^2q^2}T_{16}^{k,m}-\frac{T_{17}^{k,m}}{n}+\frac{mq'}{n^2q^2}T_{20}^{k,m}$$
$$+2\frac{m^2q'^2}{n^3q^4}T_{23}^{k,m}+\frac{m}{n^2}T_{25}^{k,m}+\frac{m}{n^2}T_{27}^{k,m}+\frac{2imq'}{n^3q^3}T_{50}^{k,m}$$
$$+\frac{i}{n^2}T_{57}^{k,m}-\frac{i}{n^2}T_{60}^{k,m},$$

$$A_m^{k,m}=-\frac{T_{17}^{k,m}}{n}-\frac{mq'}{n^2q^2}T_{20}^{k,m}+\frac{m}{n^2}T_{25}^{k,m}$$
$$+\frac{m}{n^2}T_{27}^{k,m}+\frac{T_{31}^{k,m}}{n}+\frac{i}{n^2}T_{56}^{k,m}-\frac{i}{n^2}T_{58}^{k,m},$$

$$A_{2k}^{k,m}=\frac{im}{n^2q}T_{19}^{k,m}+\frac{2im^2q'}{n^3q^3}T_{21}^{k,m}-\frac{m}{n^3q^3}$$
$$\times\left(q''-2\frac{q'^2}{q}\right)T_{23}^{k,m}-\frac{4mq'}{n^3q^3}T_{28}^{k,m}-\frac{mq'}{n^3q^3}T_{53}^{k,m},$$

$$A_{2m}^{k,m}=-\frac{im}{n^2q}T_{19}^{k,m},$$

$$A_{mk}^{k,m}=\frac{T_1^{k,m}}{q}-\frac{1}{n^2q^2}T_2^{k,m}+\frac{2im}{n^2q}T_5^{k,m}+\frac{m^2}{n^2q}T_7^{k,m}$$
$$+\frac{im}{n^2q}T_8^{k,m}-\frac{1}{n^2q}T_{14}^{k,m}+\frac{im}{n^2q}T_{15}^{k,m}+4i\frac{m^2q'}{n^3q^3}T_{21}^{k,m}$$
$$-\frac{2m}{n^3q^3}\left(q''-\frac{2q'^2}{q}\right)T_{23}^{k,m}-\frac{4mq'}{n^3q^3}T_{28}^{k,m}-\frac{2}{n^2q}T_{45}^{k,m}$$
$$+\frac{m}{n^3q^2}T_{47}^{k,m}-\frac{2m}{n^3q^2}T_{48}^{k,m}-\frac{i}{n^3q^2}T_{49}^{k,m}+\frac{k}{n^3q^2}T_{52}^{k,m}$$
$$-\frac{2mq'}{n^3q^3}T_{53}^{k,m}+\frac{i}{n^3q}T_{54}^{k,m}-\frac{1}{n^2q}T_{55}^{k,m}-\frac{1}{n^2q}T_{59}^{k,m},$$

$$A_{m2k}^{k,m}=-\frac{m^2}{n^3q^2}T_{22}^{k,m}-\frac{4im}{n^3q^2}T_{29}^{k,m}-\frac{im}{n^3q^2}T_{46}^{k,m}$$
$$+\frac{2}{n^3q^2}T_{47}^{k,m}-\frac{im}{n^3q^2}T_{51}^{k,m},$$

$$A_{2mk}^{k,m}=-\frac{m^2}{n^3q^2}T_{22}^{k,m}-\frac{2im}{n^3q^2}T_{29}^{k,m}-\frac{im}{n^3q^2}T_{46}^{k,m}$$
$$-\frac{im}{n^3q^2}T_{51}^{k,m}+\frac{2}{n^3q^2}T_{52}^{k,m},$$

$$A'^{k,m}=\frac{iqp'}{n}T_{10}^{k,m},$$

$$A_k'^{k,m}=\frac{2mq'}{n^2q^2}T_4^{k,m}+\frac{i}{n^2}T_{24}^{k,m}+\frac{i}{n^2}T_{26}^{k,m},$$

$$A_m'^{k,m}=\frac{i}{n^2}T_{24}^{k,m}+\frac{i}{n^2}T_{26}^{k,m},$$

$$A_{2k}'^{k,m}=-\frac{1}{n^2q}T_{20}^{k,m}-\frac{2mq'}{n^3q^3}T_{23}^{k,m},$$

$$A_{2m}'^{k,m}=\frac{1}{n^2q}T_{20}^{k,m},$$

$$A_{mk}'^{k,m}=-\frac{2}{n^2q}T_3^{k,m}+\frac{2im}{n^2q}T_6^{k,m}-\frac{1}{n^2q}T_{16}^{k,m}$$
$$-\frac{4mq'}{n^3q^3}T_{23}^{k,m}-\frac{2i}{n^3q^2}T_{50}^{k,m},$$

$$A_{2mk}'^{k,m}=-\frac{2im}{n^3q^2}T_{21}^{k,m}+\frac{2}{n^3q^2}T_{28}^{k,m}+\frac{1}{n^3q^2}T_{53}^{k,m},$$

$$A_{m2k}'^{k,m}=-\frac{2im}{n^3q^2}T_{21}^{k,m}+\frac{4}{n^3q^2}T_{28}^{k,m}+\frac{1}{n^3q^2}T_{53}^{k,m},$$

$$A_{mk}''^{k,m}=-\frac{1}{n^2q}T_4^{k,m},$$

$$A_{m2k}''^{k,m}=\frac{1}{n^3q^2}T_{23}^{k,m},$$

$$A_{2mk}''^{k,m}=\frac{1}{n^3q^2}T_{23}^{k,m},$$

$$I^{k,m}=-\frac{q}{f}T_{32}^{k,m}-\frac{imq}{n^2}T_{36}^{k,m}-\frac{imq}{n^2f}T_{37}^{k,m}-\frac{m^2q}{n^2f}T_{38}^{k,m}$$
$$-\frac{2im^2}{n^3}\frac{q'}{q}T_{40}^{k,m}+\frac{m}{n^3q}\left(q''-\frac{2q'^2}{q}\right)T_{41}^{k,m}-\frac{m}{n^3}T_{42}^{k,m}$$
$$+\frac{2mq'}{n^3q}T_{44}^{k,m}+\frac{q}{n^2}T_{63}^{k,m}-\frac{m}{n^3}T_{65}^{k,m}+\frac{mq'}{n^3q}T_{66}^{k,m},$$

$$I_k^{k,m}=\frac{m^2}{n^3}T_{39}^{k,m}+\frac{im}{n^3}T_{61}^{k,m}+\frac{im}{n^3}T_{64}^{k,m},$$

$$I_m^{k,m}=\frac{m^2}{n^3}T_{39}^{k,m}+\frac{im}{n^3}T_{61}^{k,m}+\frac{2im}{n^3}T_{62}^{k,m}+\frac{im}{n^3}T_{64}^{k,m},$$

$$I'^{k,m}=-\frac{2imq}{n^2f}T_{34}^{k,m}+\frac{q}{n^2}T_{35}^{k,m}+\frac{2mq'}{n^3q}T_{41}^{k,m},$$

$$I_k'^{k,m}=\frac{2im}{n^3}T_{40}^{k,m}-\frac{1}{n^3}T_{66}^{k,m},$$

$$I_m'^{k,m}=\frac{2im}{n^3}T_{40}^{k,m}-\frac{2}{n^3}T_{44}^{k,m}-\frac{1}{n^3}T_{66}^{k,m},$$

$$I''^{k,m}=\frac{q}{n^2f}T_{33}^{k,m},$$

$$I_k''^{k,m}=-\frac{1}{n^3}T_{41}^{k,m},$$

$$I_m''^{k,m}=-\frac{1}{n^3}T_{41}^{k,m}.$$

Turning now to the matrix elements involved in the boundary conditions, we have

Downloaded 14 Feb 2006 to 198.129.105.159. Redistribution subject to AIP license or copyright, see http://pop.aip.org/pop/copyright.jsp

$$S_k^{k,m} = -\frac{mq'}{nq^2} T_4^{k,m} + fp' T_{13}^{k,m} + f' T_{12}^{k,m} - \frac{i}{n} T_{24}^{k,m} - \frac{i}{n} T_{26}^{k,m},$$

$$S_{2k}^{k,m} = \frac{mq'}{n^2 q^3} T_{23}^{k,m} + \frac{1}{nq} T_{20}^{k,m},$$

$$S_{mk}^{k,m} = \frac{1}{nq} T_3^{k,m} - \frac{im}{nq} T_6^{k,m} + \frac{1}{nq} T_{18}^{k,m} + \frac{2mq'}{n^2 q^3} T_{23}^{k,m} - \frac{k}{n^2 q^2} T_{28}^{k,m} + \frac{i}{n^2 q^2} T_{50}^{k,m},$$

$$S_{m2k}^{k,m} = \frac{im}{n^2 q^2} T_{21}^{k,m} - \frac{1}{n^2 q^2} T_{28}^{k,m},$$

$$S_{2mk}^{k,m} = \frac{im}{n^2 q^2} T_{21}^{k,m} - \frac{1}{n^2 q^2} T_{28}^{k,m},$$

$$S'^{k,m}_{mk} = \frac{1}{nq} T_4^{k,m},$$

$$S'^{k,m}_{m2k} = -\frac{1}{n^2 q^2} T_{23}^{k,m},$$

$$S'^{k,m}_{2mk} = -\frac{1}{n^2 q^2} T_{23}^{k,m},$$

$$J^{k,m} = \frac{imq}{nf} T_{34}^{k,m} - \frac{mq'}{n^2 q} T_{41}^{k,m} - \frac{q}{n} T_{43}^{k,m} + \frac{m}{n^2} T_{44}^{k,m},$$

$$J_k^{k,m} = \frac{-im}{n^2} T_{40}^{k,m},$$

$$J_m^{k,m} = \frac{-im}{n^2} T_{40}^{k,m},$$

$$J'^{k,m} = -\frac{q}{nf} T_{33}^{k,m},$$

$$J'^{k,m}_k = \frac{1}{n^2} T_{41}^{k,m},$$

$$J'^{k,m}_m = \frac{1}{n^2} T_{41}^{k,m}.$$

The matrix elements $T_i^{k,m}$ are defined in terms of flux surface averages of kernels K_i

$$T_i^{k,m}(\psi) = \oint K_i(\psi,\omega) e^{i(k-m)\omega} d\omega, \tag{A3}$$

where

$$K_1 = \frac{f}{R^4 B_p^2}, \quad K_2 = q\frac{R^2 B_p^2}{JB^2}\nu'', \quad K_3 = \frac{R^2 B_p^2}{JB^2}\nu',$$

$$K_4 = \frac{fB_p^2}{B^2}, \quad K_5 = \frac{R^2 B_p^2}{JB^2}\nu'\omega', \quad K_6 = \frac{fB_p^2}{B^2}\omega',$$

$$K_7 = \frac{fB_p^2}{B^2}(\omega')^2, \quad K_8 = \frac{fB_p^2}{B^2}\omega'',$$

$$K_9 = \frac{R^2}{B^2}\frac{\partial}{\partial\psi}\left(p + \frac{B^2}{2}\right),$$

$$K_{10} = \frac{R^2}{JB^4}\frac{\partial B^2}{\partial\chi}, \quad K_{11} = \frac{R^2\omega'}{JB^4}\frac{\partial B^2}{\partial\chi}, \quad K_{12} = 1,$$

$$K_{13} = \frac{1}{B^2}, \quad K_{14} = \nu'\frac{\partial}{\partial\psi}\left(\frac{R^2 B_p^2}{JB^2}\right),$$

$$K_{15} = \nu\omega'\frac{\partial}{\partial\psi}\left(\frac{R^2 B_p^2}{JB^2}\right),$$

$$K_{16} = \nu\frac{\partial}{\partial\psi}\left(\frac{R^2 B_p^2}{JB^2}\right), \quad K_{17} = \frac{\sigma p'}{B^2}, \quad K_{18} = fp'\frac{B_p^2}{B^4},$$

$$K_{19} = \frac{f^2\sigma\omega'}{R^2B^2}, \quad K_{20} = \frac{f^2\sigma}{R^2B^2}, \quad K_{21} = \frac{f^3 B_p^2\omega'}{R^2B^4},$$

$$K_{22} = \frac{f^3\omega'^2 B_p^2}{R^2B^4}, \quad K_{23} = \frac{f^3 B_p^2}{R^2B^4}, \quad K_{24} = \frac{p'R^2B_p^2}{JB^6}\frac{\partial B^2}{\partial\chi},$$

$$K_{25} = \frac{R^2 B_p^2 p'\omega'}{JB^6}\frac{\partial B^2}{\partial\chi}, \quad K_{26} = \frac{f^2\sigma}{\nu}\frac{\partial}{\partial\chi}\left(\frac{1}{R^2B^2}\right),$$

$$K_{27} = \frac{f^2\sigma}{\nu}\frac{\partial}{\partial\chi}\left(\frac{\omega'}{R^2B^2}\right),$$

$$K_{28} = \frac{f^3 B_p^2}{R^2B^4}\frac{\nu'}{\nu}, \quad K_{29} = \frac{f^3 B_p^2}{R^2B^4}\frac{\omega'\nu'}{\nu}, \quad K_{30} = \frac{1}{\nu}\frac{\partial\sigma'}{\partial\chi},$$

$$K_{31} = \sigma', \quad K_{32} = \frac{\rho}{B_p^2}, \quad K_{33} = \frac{\rho R^4 B_p^2}{B^2},$$

$$K_{34} = \frac{\rho R^4 B_p^2\omega'}{B^2}, \quad K_{35} = \frac{1}{\nu}\frac{\partial}{\partial\psi}\left(\frac{\rho JR^2B_p^2}{B^2}\right),$$

$$K_{36} = \frac{\omega'}{\nu}\frac{\partial}{\partial\psi}\left(\frac{\rho JR^2B_p^2}{B^2}\right),$$

$$K_{37} = \frac{\rho R^4 B_p^2\omega''}{B^2}, \quad K_{38} = \frac{\rho R^4 B_p^2\omega'^2}{B^2}, \quad K_{39} = H\omega'^2,$$

$$K_{40} = H\omega', \quad K_{41} = H, \quad K_{42} = \frac{H\nu''}{\nu},$$

$$K_{43} = \frac{G}{\nu}, \quad K_{44} = \frac{H\nu'}{\nu}, \quad K_{45} = \frac{f^3 B_p^2}{R^2B^4}\left(\frac{\nu'}{\nu}\right)^2,$$

$$K_{46} = \frac{f^3 B_p^2\omega''}{R^2B^4}, \quad K_{47} = \frac{f^3 B_p^2}{R^2B^4}\frac{\nu''}{\nu},$$

$$K_{48} = \frac{f^3\omega'\nu'}{\nu}\frac{\partial}{\partial\omega}\left(\frac{B_p^2}{R^2B^4}\right), \quad K_{49} = \frac{f^3\nu''}{\nu}\frac{\partial}{\partial\omega}\left(\frac{B_p^2}{R^2B^4}\right),$$

$$K_{50} = \frac{f^3\nu'}{\nu}\frac{\partial}{\partial\omega}\left(\frac{B_p^2}{R^2B^4}\right), \quad K_{51} = \nu^2\omega'\frac{\partial}{\partial\psi}\left(\frac{f^3 B_p^2}{\nu^2R^2B^4}\right),$$

Downloaded 14 Feb 2006 to 198.129.105.159. Redistribution subject to AIP license or copyright, see http://pop.aip.org/pop/copyright.jsp

$$K_{52}=\nu\nu'\frac{\partial}{\partial\psi}\left(\frac{f^3B_p^2}{\nu^2R^2B^4}\right),\quad K_{53}=\nu^2\frac{\partial}{\partial\psi}\left(\frac{f^3B_p^2}{\nu^2R^2B^4}\right),$$

$$K_{54}=\nu\frac{\partial}{\partial\psi}\left(\frac{f^3B_p^2}{\nu^2R^2B^4}\right)\frac{\partial}{\partial\chi}\left(\frac{\nu'}{\nu}\right),$$

$$K_{55}=\nu\frac{\partial}{\partial\psi}\left(\frac{fp'B_p^2}{\nu B^4}\right),\quad K_{56}=\frac{p'R^2B_p^2}{JB^6}\frac{\nu'}{\nu}\frac{\partial B^2}{\partial\chi},$$

$$K_{57}=\frac{\partial}{\partial\psi}\left(\frac{p'R^2B_p^2}{JB^6}\frac{\partial B^2}{\partial\chi}\right),$$

$$K_{58}=\frac{f^2p'}{JB^6}\frac{\nu'}{\nu}\frac{\partial B^2}{\partial\chi},\quad K_{59}=\nu\frac{\partial}{\partial\psi}\left(\frac{f\sigma}{JB^2}\right),$$

$$K_{60}=\frac{\partial}{\partial\psi}\left(\frac{f^2p'}{JB^6}\frac{\partial B^2}{\partial\chi}\right),\quad K_{61}=H\omega'',\quad K_{62}=\frac{\omega'\nu'}{\nu}H,$$

$$K_{63}=\frac{1}{\nu}\frac{\partial G}{\partial\psi},\quad K_{64}=\omega'\frac{\partial H}{\partial\psi},\quad K_{65}=\frac{\nu'}{\nu}\frac{\partial H}{\partial\psi},$$

$$K_{66}=\frac{\partial H}{\partial\psi}.$$

Here we have defined two additional variables, dependent upon the equilibrium

$$H=\frac{\rho fR^2B_p^2}{B^4} \tag{A4}$$

and

$$G=\frac{\rho R^2JB_p^2}{B^2}\left(\frac{p'}{B^2}+\frac{\nu'}{\nu}\frac{f^2}{R^2B^2}\right). \tag{A5}$$

Note that a prime denotes a derivative with respect to ψ, and ρ is the plasma mass density.

APPENDIX B: EQUILIBRIUM RADIAL VARIATION

The first task of ELITE is to analyze the equilibrium and evaluate the matrix elements described in Appendix A. It is convenient to calculate these matrix elements on each flux surface in turn, without reference to other equilibrium flux surfaces in their neighborhood. It is therefore necessary to be able to evaluate radial derivatives on a flux surface in terms of only the equilibrium parameters on that flux surface. This is made possible through the technique of expanding the equilibrium locally about that flux surface, using the information provided by the Grad–Shafranov equation, as described in Ref. 12, for example.

Thus, following Ref. 12, we express:

$$\psi=\psi_0+\psi_1(l)r+\psi_2(l)r^2+\psi_3(l)r^3+\cdots, \tag{B1}$$

where l is the distance around the flux surface labeled ψ_0 in the poloidal cross-section and r is the radial distance from that flux surface (see Ref. 12). Although we need to expand to higher order than was done in Ref. 12 (as we need to evaluate second derivatives with respect to ψ), the technique is basically the same. We, therefore, do not describe it in detail, but simply quote some useful results. Thus, by substituting the above form for ψ into the Grad–Shafranov equation and equating powers in r, we find

$$\psi_1(l)=R_s(l)B_{ps}(l), \tag{B2}$$

$$\psi_2(l)=\frac{1}{2}\left[\left(\frac{R_s}{R_c}+\sin u\right)B_{ps}-R_s^2p'-ff'\right], \tag{B3}$$

$$\begin{aligned}\psi_3(l)=\frac{1}{6}\Bigg[&-2B_{ps}\sin u\left(\frac{1}{R_c}+\frac{\sin u}{R_s}\right)\\&+4\psi_2\left(\frac{1}{R_c}+\frac{\sin u}{R_s}\right)-R_s\frac{\partial}{\partial l}\left(\frac{1}{R_s}\frac{\partial\psi_1}{\partial l}\right)\\&+R_s^2p'\left(\frac{1}{R_c}-\frac{\sin u}{R_s}\right)+ff'\left(\frac{1}{R_c}+\frac{\sin u}{R_s}\right)\\&-R_sB_{ps}(R_s^2p''+(ff')')\Bigg].\end{aligned} \tag{B4}$$

All quantities are to be evaluated on the reference flux surface, $\psi=\psi_0$ (the subscript s on some of the variables denotes this). The angle u is defined by $dR_s/dl=\cos u$, $dZ_s/dl=-\sin u$ and R_c is the radius of curvature, which can also be defined in terms of u: $du/dl=-R_c^{-1}$.

Now that we know ψ to sufficiently high order we can evaluate the equilibrium quantities required by ELITE. In particular, we have

$$RB_p=R_sB_{ps}\left[1+2r\frac{\psi_2}{\psi_1}+\frac{r^2}{2}\left[\frac{6\psi_3}{\psi_1}+\frac{1}{\psi_1^2}\left(\frac{\partial\psi_1}{\partial l}\right)^2\right]\right], \tag{B5}$$

for the poloidal magnetic field, where

$$R=R_s(l)+r\sin u. \tag{B6}$$

Another important quantity is ν, as the derivatives of this are required in order to derive q' and q''. Thus we need to evaluate ν to $O(r^2)$, and Eq. (B5) is required to provide this. Thus we express

$$\nu=\nu_s(1+\nu_1r+\nu_2r^2+\cdots)\frac{f(\psi)}{f(\psi_0)}, \tag{B7}$$

where

$$\nu_1=-\frac{1}{R_c}-\frac{\sin u}{R_s}-\frac{2\psi_2}{\psi_1}, \tag{B8}$$

$$\nu_2=\left(\frac{\sin u}{R_s}+\frac{2\psi_2}{\psi_1}\right)\left(\frac{1}{R_c}+\frac{\sin u}{R_s}\right)-\frac{3\psi_3}{\psi_1}+\frac{4\psi_2^2}{\psi_1^2}. \tag{B9}$$

[1] J. W. Connor, R. J. Hastie, and J. B. Taylor, Proc. R. Soc. London, Ser. A **A365**, 1 (1979).
[2] D. Lortz, Nucl. Fusion **15**, 49 (1975).
[3] J. A. Wesson, Nucl. Fusion **18**, 87 (1978).
[4] J. W. Connor, R. J. Hastie, H R. Wilson, and R. L. Miller, Phys. Plasmas **5**, 2687 (1998).
[5] C. C. Hegna, J. W. Connor, R. J. Hastie, and H. R. Wilson, Phys. Plasmas **3**, 584 (1996).
[6] H. R. Wilson and R. L. Miller, Phys. Plasmas **6**, 873 (1999).
[7] H. Zohm, Plasma Phys. Controlled Fusion **38**, 1213 (1996).
[8] R. Aymar, Plasma Phys. Controlled Fusion **42**, B385 (2000).
[9] A. B. Mikhailovskii, G. T. A. Huysmans, W. O. K. Kerner, and S. E. Sharapov, Plasma Phys. Rep. **23**, 844 (1997).

Downloaded 14 Feb 2006 to 198.129.105.159. Redistribution subject to AIP license or copyright, see http://pop.aip.org/pop/copyright.jsp

[10]L. L. Lao, H. St. John, R. D. Stambaugh, A. G. Kellman, and W. Pfeiffer, Nucl. Fusion **25**, 1611 (1985).
[11]J. P. Freidberg, *Ideal Magnetohydrodynamics* (Plenum, New York, 1987), pp. 256–257.
[12]R. L. Miller, M. S. Chu, J. M. Greene, Y. R. Lin-Liu, and R. L. Waltz, Phys. Plasmas **5**, 973 (1998).
[13]H. R. Wilson, P. B. Snyder, and G. T. A. Huysmans, to appear in *Proceedings of the 28th European Physical Society Conference on Controlled Fusion and Plasma Physics*, Madeira (European Physical Society, 2001).
[14]P. B. Snyder, H. R. Wilson, J. R. Ferron *et al.*, Phys. Plasmas (to be published).
[15]R. J. Hastie, P. J. Catto, and J. J. Ramos, Phys. Plasmas **7**, 4561 (2000).
[16]G. T. A. Huysmans, S. E. Sharapov, and A. B. Mikhailovskii, *Proceedings of the 27th European Physical Society Conference on Controlled Fusion and Plasma Physics Budapest* (European Physical Society, Petit-Lancy, 2000), p. 1072.
[17]G. T. A. Huysmans, S. E. Sharapov, A. B. Mikhailovskii, and W. Kerner, Phys. Plasmas **8**, 4292 (2001).

Downloaded 14 Feb 2006 to 198.129.105.159. Redistribution subject to AIP license or copyright, see http://pop.aip.org/pop/copyright.jsp